Delft University of Technology

Optimization of virtually aperiodic linear sparse arrays

Aslan, Yanki

Important note
To cite this publication, please use the final published version (if applicable).
Please check the document version above.

RESEARCH ARTICLE

WILEY

Optimization of virtually aperiodic linear sparse arrays

Yanki Aslan

Department of Microelectronics, Microwave Sensing, Signals and Systems Group, Delft University of Technology, Delft, The Netherlands

Correspondence
Yanki Aslan, Department of Microelectronics, Microwave Sensing, Signals and Systems Group, Delft University of Technology, HB 21, Mekelweg 4, 2628 CD Delft, The Netherlands.
Email: y.aslan@tudelft.nl

Abstract

Multi-port multi-mode antenna elements have the ability to move their phase centers and modify their radiation patterns electronically. Arrays composed of such elements are referred to as virtually aperiodic arrays in this paper. Herein, optimization of the mode excitation coefficients in virtually aperiodic sparse linear arrays is proposed, by introducing novel design constraints with the aim of synthesizing wide-angle scanning, reconfigurable patterns, with grating/side lobe reduction. A dual-mode patch antenna is used for demonstration purposes. An efficient convex optimization based algorithm is adopted to optimize the excitation weight at each element mode port, while considering the mutual coupling effects. Through full-wave simulations, the effectiveness of the optimization in suppressing the unwanted radiation and adapting to different fields-of-view is shown. A novel investigation on the impacts of defining different mode excitation ratios on the radiation pattern characteristics is conducted.

KEYWORDS

antenna synthesis, array optimization, grating lobes, multi-mode antennas, phased arrays, sparsity

1 | INTRODUCTION

Aperiodic arrays have been widely studied in the literature for various applications including satellite communications,[1] cellular communications,[2] wireless power transfer,[3] radars for imaging[4] and direction-of-arrival estimation.[5] Compared to the periodic counterparts, they can further decrease the level of high side lobes, dissolve the grating lobes in the case of sparse arrays, improve the beam resolution, provide more space for the beamformer electronics and enhance the thermal performance.[6] Despite the listed advantages, physically aperiodic arrays have several limitations and drawbacks. First, the unique array layout is designed to satisfy a specific pattern mask depending on the field-of-view, side lobe requirements, aperture size and desired average element spacing.[7] Therefore, each array becomes use-case specific with no reconfigurability in its layout for different pattern requirements, unless there are some movable mechanical parts that can rearrange the element positions.[8] However, implementing such movable units increases the system complexity, creates reliability issues and prevents fast operation. Second, aperiodic arrays generally result in an increase in the array size. This is due to the increased sparsity at the peripheral region.[9] Third, due to the asymmetry, the feed network design may become much more complex when compared to the periodic arrays, which in turn increases the losses and calibration requirements.[10,11]

The disadvantages and challenges brought by the physically aperiodic arrays motivate the search for ways of realizing the aperiodicity electronically (i.e., virtual aperiodicity). This can be ideally achieved by controlling the phase center of each element separately, which determines the relative position of the elements in the array. For a microstrip antenna element, a smart approach to control the phase center is to excite multiple modes (fundamental mode and higher order mode[s]).[12] If the antenna functions at a single mode, the phase center will coincide with its physical center. However, combination of two or more modes helps move the phase center away. The new phase center (as well as the modifications in the pattern shape and polarization properties) is determined by the relative amplitude and phase excitations of the modes.[13,14]

The concept of electronic control of the element phase center and radiation pattern via multi-mode excitation has already been established. However, the idea of exploiting this concept to achieve adaptive element spacing for electronic pattern reconfigurability was only proposed very recently,[15] where only small (2- and 3-element) arrays radiating at broadside are considered. There are also a few recent works that demonstrated the grating lobe reduction capability of the multi-mode excitation technique in phased arrays

(with seven elements arranged in a linear or hexagonal topology) having a large element spacing.[16,17] However, they aim to modify the (common) element pattern (which is to be multiplied by the array factor) so as to achieve sufficient gain toward the scanning angle, while placing a null at the angle of the grating lobe.

In the case of multi-port multi-mode excitation for null-scanning, a constant 90-degree phase shift is used between the two ports of each element.[16,17] The common amplitude ratio at the two ports of each element, and the excitation amplitude ratio between the center element and the peripheral elements are found via an extensive search routine. A primitive study toward optimizing the excitation coefficients was also conducted.[18] However, (i) the analysis was based on simplified analytical expressions for radiation, (ii) there was no control on the amplitude ratio between the fundamental and higher order mode, which can cause a significant reduction in the array gain, (iii) only normalized radiation patterns were considered that do not reflect the absolute gain values, (iv) there were no constraints on the beamwidth and input power and (v) there was no consideration of pattern reconfigurability. Thus, it can be inferred that the existing approaches do not carefully use the full synthesis flexibility in terms of individual amplitude-phase control at each port in the array, do not guarantee the optimality of the solution, do not consider mutual coupling effects in the synthesis, and cannot adapt to the changes in the beam forming requirements fast enough.

A more ambitious aim would be to apply this concept to phased arrays with a larger number of elements, and to optimize the mode excitation coefficients efficiently at each element using a desired (and reconfigurable) goal function on the array radiation pattern, while including the mutual coupling effects. In that way, full electronic control (position and radiation pattern) at each element could be achieved. To this aim, this paper proposes a novel optimization methodology in electronically reconfigurable, wide-angle scanning, virtually aperiodic sparse linear array synthesis for effective side lobe/grating lobe suppression. To the author's knowledge, this is the first time that optimization of virtually aperiodic phased arrays is studied comprehensively with novel and practical design constraints. The proposed concept is particularly interesting for the applications where sparsity in the array layout is desired. A recent and relevant example is active millimeter-wave phased array antennas for beyond-5G, for which the high potential of using large inter-element spacings is extensively reported in the literature in terms of improved spatial multiplexing,[19,20] antenna-IC (Integrated Circuit) integration[21] and thermal management.[22]

The rest of the paper is organized as follows. The design details for the multi-mode antenna element and its array used for demonstration purposes are provided in section 2. The optimization procedure is explained in section 3. The simulation settings, results and complementary discussions are given in section 4. The conclusions are reported in section 5.

2 | ANTENNA ELEMENT AND ARRAY

Let us consider a stacked circular patch antenna element with two ports. The first port feeds the upper patch with smaller radius and excites the fundamental (TM_{11}) mode, while the second port feeds the lower patch with larger radius and excites the high order (TM_{21}) mode. The feed points are located along the horizontal axis (i.e., x-axis). In order to control each mode separately, the lower patch is used as the ground plane for the upper patch.[23] The design parameters' values were estimated by following the cavity-model based design strategy for the patch radii[24] and the best ratio of feed location to disk radius analysis.[25] Considering the impact of coupling, further tuning based on full-wave simulations was then applied to satisfy the matching requirements at the center frequency of 9 GHz.

The dual-mode element design and its array are shown in Figure 1. Both the upper and lower patch substrates have the relative permittivity of 2.2. The values of all the design
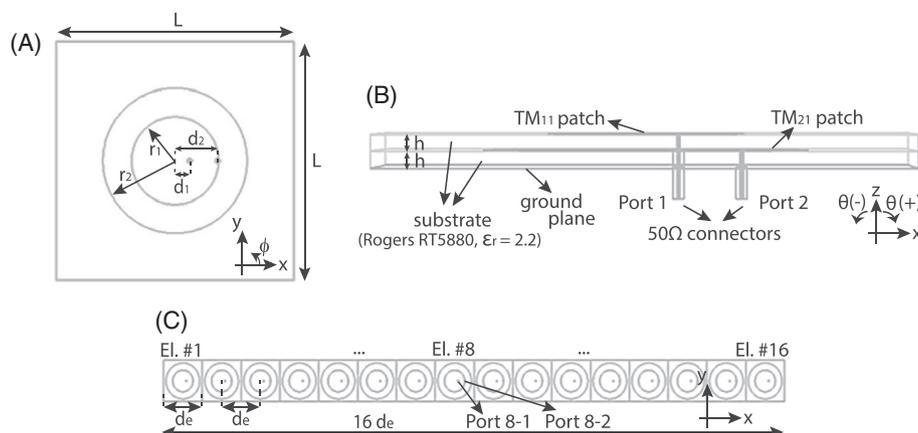
FIGURE 1 Design of the dual-mode antenna: (A) element top view, (B) element side view, (C) array top view

parameters are listed as follows: $f_0 = 9$ GHz, $r_1 = 6.10$ mm, $r_2 = 10.13$ mm, $d_1 = 2.05$ mm, $d_2 = 5.98$ mm, $L = 23.33$ mm ($0.7 \lambda_0$), $h = 1$ mm, $d_e = 23.33$ mm ($0.7 \lambda_0$). In the array, the first (TM_{11}) port of the nth element is labeled as "Port $n-1$," while the second (TM_{21}) port of the nth element is labeled as "Port $n-2$."

3 | OPTIMIZATION PROCEDURE

The co-polarized electric far-field radiated by an N-element linear array arranged as shown in Figure 1 with dual-mode, dual-port elements for a scanned beam s, $f^s(\theta)$, is given by

$$f^s(\theta) = \sum_{n=1}^{N} \left(e_{n,1}(\theta) \, w_n^s + e_{n,2}(\theta) \, q_n^s \right) \quad (1)$$

where $e_{n,1}(\theta)$ and $e_{n,2}(\theta)$ denote the complex horizontally polarized (in Ludwig-3 definition) embedded electric far-fields with respect to the array origin for the excitation of first port and second port of the nth element in the array, respectively. The complex valued coefficients w_n^s and q_n^s represent the excitation weights of the nth element for the scanned beam s for the first (TM_{11}) and the second (TM_{21}) ports, respectively.

In this work, the goal function considered for optimization of excitation weights w_n^s and q_n^s is to minimize the peak magnitude of radiation outside the main lobe for a wide-angle scan. To achieve this, the set of observation angles θ corresponding to region outside the main lobe for each scanned beam s should be stored. A straightforward way to achieve this is to define a main lobe beam width θ_b such that

$$\theta \in \boldsymbol{\theta}_c^s \text{ if } \left[-\theta_h \leq \theta < \left(\theta_0^s - \theta_b\right)\right] \text{ or } \left[\theta_h \geq \theta > \left(\theta_0^s + \theta_b\right)\right] \quad (2)$$

where θ_0^s is the angle of the main lobe maximum for the scanned beam s, and θ_h is the largest observation angle in the angular region-of-interest. The vector $\boldsymbol{\theta}_c^s$ holds the set of observation angles outside the main lobe of the scanned beam s. Here, the same θ_b value is used for all the scanned beams, but it can be varied with increased scan angles.

The complete optimization problem for a scanned beam s at a single frequency can be formulated as

$$\text{minimize } \rho_{\max}^s, \quad \text{for} \begin{cases} |f^s(\theta)| \leq \rho_{\max} \text{ for } \theta \in \boldsymbol{\theta_c^s}, \\ w_1^s = 1, \\ |w_n^s| \leq w_{\max}, \ \forall n \in [1, \cdots, N] \\ |q_n^s| \leq q_{\max}, \ \forall n \in [1, \cdots, N] \end{cases} \quad (3)$$

where $\rho_{\max}^s$ (to be minimized) is the maximal magnitude of the electric field outside the main lobe for the scanned beam s. The parameters $w_{\max}$ and $q_{\max}$ can be used to put upper limits on the excitation magnitudes for the first and second ports at each element, respectively. The excitation amplitude at the first port of the first element is equal to 1 for all the scanned beams, which is used as a reference (since otherwise, all the weights will be set to zero to minimize $\rho_{\max}^s$).

The optimization problem in (3) is a convex problem,[26] which can be efficiently solved by using the Interior Point Method[27] based solvers available in the existing optimization software packages.[28] Obtaining the solution to (3) with several iterations for convergence takes only about half a second in a standard laptop, which can be shortened in the case of a more powerful processor. After the optimization is done, an additional constraint is applied to ensure the total transmit power is equal to 1 for a fair comparison between the various cases analyzed in the next section, which results in

$$\begin{aligned} w_n'^s &= w_n^s \Big/ \sqrt{\sum_{n=1}^{N} \left(|w_n^s|^2 + |q_n^s|^2 \right)} \\ q_n'^s &= q_n^s \Big/ \sqrt{\sum_{n=1}^{N} \left(|w_n^s|^2 + |q_n^s|^2 \right)} \end{aligned} \quad (4)$$

where $w_n'^s$ and $q_n'^s$ are the excitation coefficients scaled according to the power constraint.

4 | SIMULATION SETTINGS, RESULTS AND DISCUSSION

The embedded element gain patterns for the horizontal polarization for each element and for each port are plotted in Figure 2 for varying observation angles at 9 GHz. The observed patterns for Port 1 (TM_{11}, maximum at broadside) and Port 2 (TM_{21}, null at broadside) are in line with the theory. Some variations from element-to-element can be observed, which originates from the mutual coupling. The complex embedded far-fields are then combined in array pattern synthesis after being multiplied by the scaled excitation coefficients ($w_n'^s, q_n'^s$) corresponding to them.

Initially, the array patterns with scanning for two reference cases are computed. In the reference cases, only single dominant mode (TM_{11}) excitation is considered (i.e., $q_n'^s = 0, \forall s, n$) for 7 scan angles from -45 degrees to 45 degrees with 15 degree steps. As for the values of $w_n'^s$, uniform amplitudes and 30 dB Chebyshev window amplitude taper are applied with linearly progressive phases. Table 1 (first two array types) shows the array gain and side lobe peaks for horizontal polarization with scanning. It is seen that although side lobes are effectively suppressed by the tapering, the problem with grating lobes is observed as expected in both cases when $|\theta_0^s| = 30, 45$ degrees.

Having the reference results at hand, next the pattern results with optimized port excitation coefficients at the 9 GHz operation frequency will be provided and discussed. The optimization settings used in the formulation of the problem in (3) are as follows:
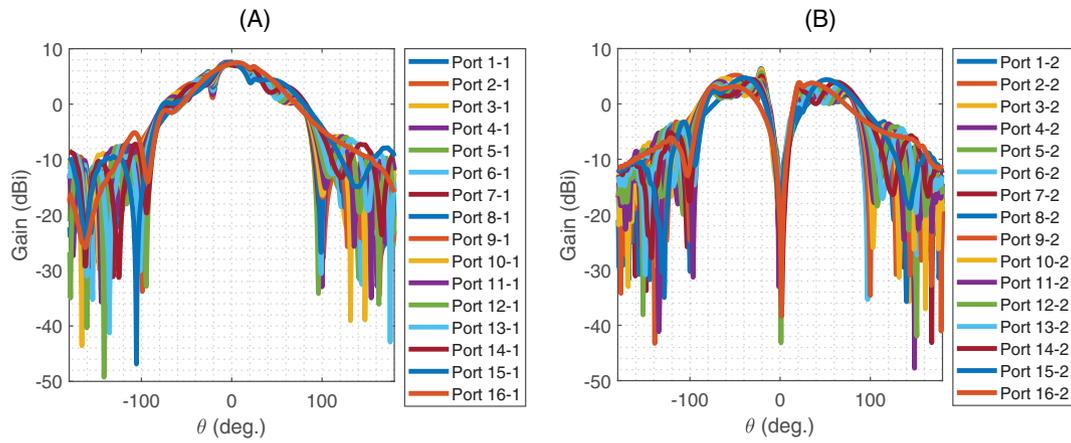
FIGURE 2 Embedded element realized gain patterns for horizontal polarization in the 16-element linear array at 9 GHz for the excitation of: (A) first port at each element, (B) second port at each element [Color figure can be viewed at wileyonlinelibrary.com]

TABLE 1 A summary of 16-element linear array optimization results at 9 GHz in terms of the main beam peak and side/grating lobe peak realized gain levels for different array types and different main beam positions

Array type	Main beam position (deg.)	Main beam peak (dBi)	Side (or grating) lobe peak (dBi)
Uniformly fed	−45	14.6	15.0
	−30	16.5	13.2
	−15	18.1	5.9
	0	19.3	6.0
	15	18.5	5.9
	30	17.0	11.9
	45	15.1	14.5
30 dB Chebwin tapered	−45	14.0	14.3
	−30	15.9	12.5
	−15	17.5	−11.1
	0	18.7	−11.4
	15	17.8	−12.2
	30	16.4	11.2
	45	14.5	13.8
Optimized, $q_{max} = 0.5$	−45	13.8	−4.4
	−30	16.1	−5.6
	−15	16.9	−14.8
	0	18.0	−15.5
	15	16.6	−15.6
	30	16.2	−7.2
	45	13.9	−5.4
Optimized, $q_{max} = 1$	−45	9.6	−10.7
	−30	14.7	−11.9
	−15	15.4	−16.5
	0	16.6	−17.1
	15	14.8	−17.5

TABLE 1 (Continued)

Array type	Main beam position (deg.)	Main beam peak (dBi)	Side (or grating) lobe peak (dBi)
	30	13.5	−13.5
	45	9.9	−11.1

- $\theta_0^s = [−45, −30, −15, 0, 15, 30, 45]$ degrees
- $\theta_h = 90$ degrees
- $\theta_b = 8$ degrees
- w_{max}: not defined
- q_{max}: varied, $= [0.5, 1]$
- θ step size $= 0.5$ degrees

The realized gain patterns and optimized excitation coefficients are provided in Figure 3 and Figure 4 for $q_{max} = 0.5$ and $q_{max} = 1$, respectively. It is worth to mention that to keep the readability of the graphs, only the excitation coefficients for $\theta_0^s = [15, 30, 45]$ degrees are shown. The optimization results in terms of the peak realized gains at the desired beam positions and side (or grating) lobe peak gains within the angular region-of-interest are summarized in Table 1 (last two array types).

From the optimization results, the following main observations can be made:

1. When $q_n'^s = 0$, $\forall s, n$ (i.e., TM_{21} mode is not excited), the problem with grating lobes cannot be solved via optimization.
2. When the second ports at each element are excited for multi-mode operation, the grating lobes are suppressed by about 20 dB on average for varied q_{max} values.
3. The relative side lobe peak remains below about −32 dB for the non-zero q_{max} values chosen for radiation near broadside (i.e., $\theta_0^s = [−15, 0, 15]$ degrees).
4. Excitation of the TM_{21} mode generally reduces the array gain at the beam peaks as compared to the reference
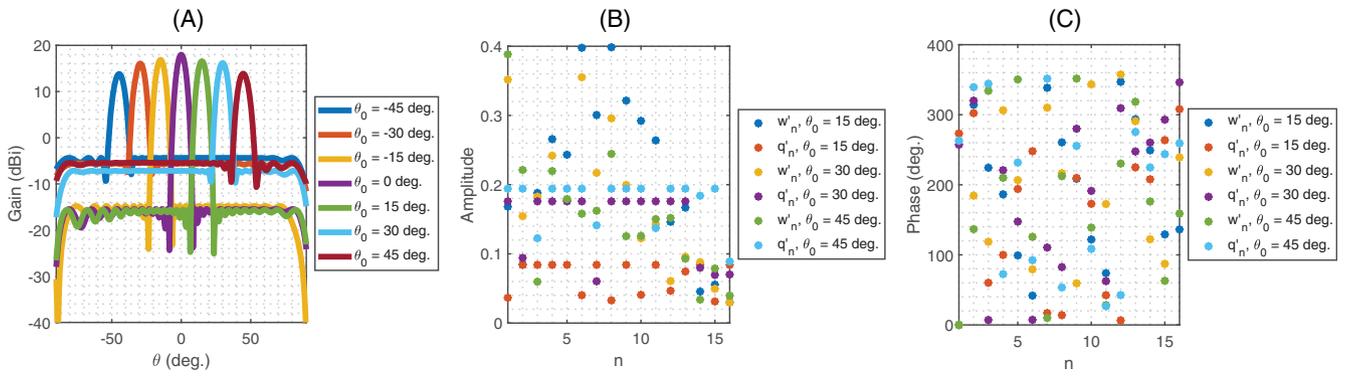
FIGURE 3 Results of optimization of excitation coefficients $(w_n^{\prime s}, q_n^{\prime s})$ in the 16-element linear array at 9 GHz for ± 45 degree scanning with 15-degree steps when $q_{max} = 0.5$: (A) realized gains for horizontal polarization, (B) excitation amplitudes, (C) excitation phases [Color figure can be viewed at wileyonlinelibrary.com]
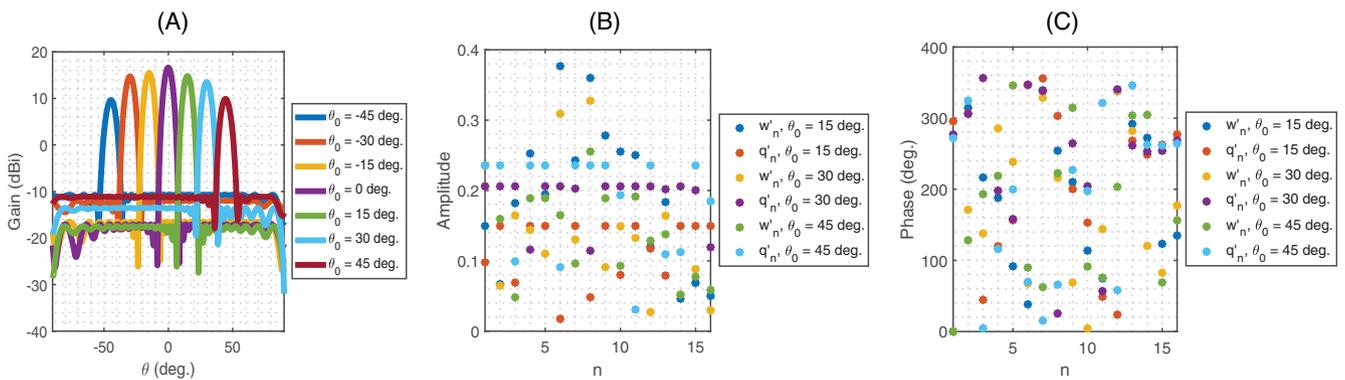
FIGURE 4 Results of optimization of excitation coefficients $(w_n^{\prime s}, q_n^{\prime s})$ in the 16-element linear array at 9 GHz for ± 45 degree scanning with 15-degree steps when $q_{max} = 1$: (A) realized gains for horizontal polarization, (B) excitation amplitudes, (C) excitation phases [Color figure can be viewed at wileyonlinelibrary.com]
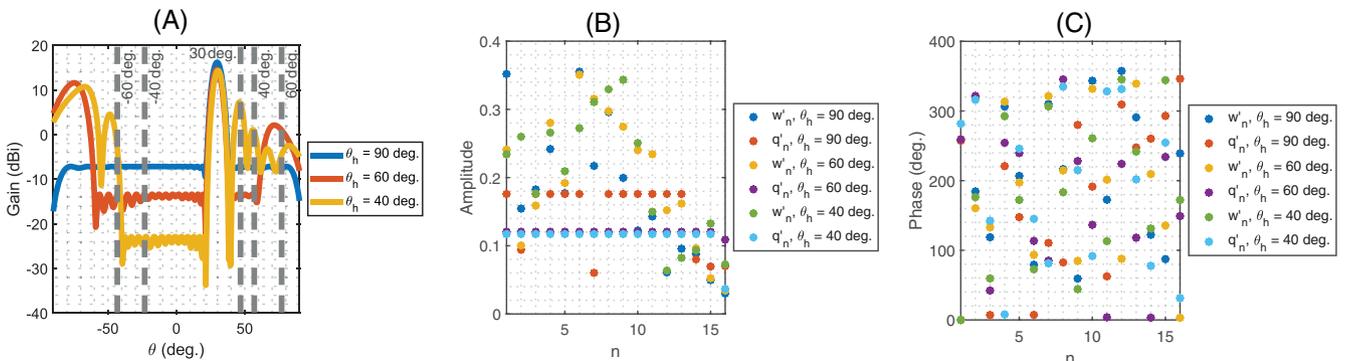
FIGURE 5 Results of optimization of excitation coefficients $(w_n^{\prime s}, q_n^{\prime s})$ in the 16-element linear array at 9 GHz for 30 degree scanning when θ_h = [90 60 40] degrees, $q_{max} = 0.5$: (A) realized gains for horizontal polarization, (B) excitation amplitudes, (C) excitation phases [Color figure can be viewed at wileyonlinelibrary.com]

cases. The extent of reduction depends on the ratio of this mode with respect to the TM_{11} mode, which is controlled by the parameter q_{max} in the optimization model. For $q_{max} = 0.5$, the maximum decrease in the beam peak within the ± 45 degree scan range is only about 1 dB as compared to the 30 dB Chebwin tapered reference array. On the other hand, for $q_{max} = 1$, the beam peak reduction reaches up to 4.6 dB as compared to the tapered reference array, which is seen for the beam at 45 degrees.

5. There is a trade-off between the grating lobe suppression capability and the array gain. For example, for the

outermost scanned beam at −45 degrees, the grating lobe is reduced by about 18 and 20 dB for $q_{max} = 0.5$ and 1, respectively. The final selection of q_{max} can be made based on the system requirements.

Next, an additional study case is performed to demonstrate the usefulness of the proposed optimization routine with reconfigurability to different angular region-of-interests. Let us consider the beam scanned to 30 degrees. The parameter θ_h is varied. Thus, the optimizer aims to minimize the grating/side lobes within the modified region-of-interest.

The following settings are used for the optimization:

• $\theta_0^s = 30$ degrees	• w_{max}: not defined
• θ_h: varied, = [90, 60, 40] degrees	• $q_{max} = 0.5$
• $\theta_b = 8$ degrees	• θ step size = 0.5 degrees

The realized gain patterns and excitation coefficient results at 9 GHz are shown in Figure 5. The outcome in terms of array gain at 30 degrees and side/grating lobe peak gains within $\pm\theta_h$ is summarized as follows: for $\theta_h = 90, 60, 40$ deg., main beam peak is 16.2, 14.5, 14.3 dBi and the side (or grating) lobe peak within $\pm\theta_h$ is −7.2, −13.4, −22.9 dBi, respectively.

From these results, it can be inferred that at the expense of some reduction in the peak array gain, the excitation coefficients can be reconfigured to further suppress the unwanted radiation within the $\pm\theta_h$ range, which increases the radiation outside the region-of-interest. The suppression becomes more effective while θ_h decreases. For example, when θ_h is changed from 90 degrees to 40 degrees, the gain at 30 degrees reduces by 1.9 dB, while the side lobe peak gain within $\pm\theta_h$ is reduced by 15.7 dB.

Note that in general, the cross-polarization level increases with the increasing ratio of the TM_{21} mode as compared to the TM_{11} mode.[29] One way to reduce the cross-polarization levels is to modify the structure by adding another layer to the bottom with a larger patch and a separate (third) port which excites the TM_{02} mode. Since this mode provides an omnidirectional pattern in azimuth, adding a proper amount of the TM_{02} mode to the TM_{11} and TM_{21} modes can help reduce the cross polarization, as demonstrated in the literature.[29] Excitation and optimization of more than two modes is out-of-scope of the paper.

5 | CONCLUSIONS

In this paper, the idea of optimizing the excitation coefficients in arrays with multi-port multi-mode antenna elements (i.e., virtually aperiodic arrays) for low side/grating lobe patterns in a wide scanning range and for pattern reconfigurability has been proposed and investigated comprehensively for the first time.

Through comparative simulation and optimization results with respect to the reference arrays using dominant mode excitation only, the capabilities/limitations of virtually aperiodic arrays in suppressing the grating lobes in wide-angle scanning and maintaining the beam peak levels have been identified. Moreover, the trade-offs between the grating lobe suppression capability and peak field magnitude decrease have been studied by using various higher mode excitation ratios in the optimizer. It has been inferred that by constraining the higher mode ratio to a relatively low (but non-zero) value, the grating lobes can be suppressed very effectively, while maintaining close-to-optimum field magnitudes. The reconfigurability for narrower field-of-views has provided further unwanted radiation suppression capability in the field-of-view, which comes at the expense of slight reduction in the beam peak and increased radiation outside the field-of-view.

The future work will focus on identifying the capabilities of the optimization in planar arrays with phase center/radiation pattern control in both array dimensions, and on addressing the polarization/gain loss and bandwidth requirements with different approaches to element design and array optimization.

ORCID

Yanki Aslan https://orcid.org/0000-0002-6834-8375

REFERENCES

[1] Bencivenni C, Ivashina MV, Maaskant R, Wettergren J. Synthesis of maximally sparse arrays using compressive sensing and full-wave analysis for global earth coverage applications. *IEEE Trans. Antennas Propag.* 2016;64(11):4872-4877.

[2] Ge X, Zi R, Wang H, Zhang J, Jo M. Multi-user massive MIMO communication systems based on irregular antenna arrays. *IEEE Trans Wirel Commun.* 2016;15(8):5287-5301.

[3] Li X, Duan B, Zhou J, Song L, Zhang Y. Planar array synthesis for optimal microwave power transmissionwith multiple constraints. *IEEE Antennas Wirel Propag Lett.* 2017;16:70-73.

[4] Wang J, Aubry P, Yarovoy A. 3-D short-range imaging with irregular MIMO arrays using NUFFT-based range migration algorithm. *IEEE Trans Geosci Remote Sens.* 2020;58(7):4730-4742.

[5] Shakeri S, Ariananda DD, Leus G. Direction of arrival estimation using sparse ruler array design. In: Proc. 13th IEEE SPAWC; 2012:525-529.

[6] Rocca P, Oliveri G, Mailloux RJ, Massa A. Unconventional phased Array architectures and design methodologies—a review. *Proc IEEE*. 2016;104(3):544-560.

[7] Aslan Y, Puskely J, Roederer A, Yarovoy A. Trade-offs between the quality of service, computational cost and cooling complexity in interference-dominated multi-user SDMA systems. *IET Comm*. 2020;14(1):144-151.

[8] Anjos E, SalarRahimi M, Bressner T, et al. FORMAT: a reconfigurable tile-based antenna Array system for 5G and 6G millimeter-wave testbeds. *IEEE Sys J*. 2021.

[9] Aslan Y, Roederer A, Yarovoy A. System advantages of using large-scale aperiodic Array topologies in future mm-wave 5G/6G base stations: an interdisciplinary look. *IEEE Sys. J. Early Access*. 2021;1-10.

[10] Kibaroglu K, Sayginer M, Rebeiz GM. A scalable 64-element 28 Ghz phased-array transceiver with 50 dBm EIRP and 8–12 Gbps 5G link at 300 meters without any calibration. In: Proc. IEEE/MTT-S IMS; 2018:496-498.

[11] Camps MB. Design of a Sparse Irregular Array for beyond 5G Base Stations [Master's thesis]. Delft University of Technology. Delft, The Netherlands; 2021.

[12] Pour ZA, Shafai L. Control of phase center and polarization in circular microstrip antennas. In: Proc. IEEE APS-URSI; 2006:1441-1444.

[13] Pour ZA, Shafai L, Mehrabani A. Virtual array antenna with displaced phase centers for GMTI applications. In: Proc. IEEE RadarCon (RADAR); 2011;830-834.

[14] Pour ZA, Shafai L. Adaptive aperture antennas with adjustable phase centre locations. In: Proc. IEEE iWAT; 2012:355-357.

[15] Mitha T, Pour M. Principles of adaptive element spacing in linear array antennas. *Nat Sci Rep*. 2021;11(1):1-11.

[16] Iqbal Z, Pour M. Grating lobe reduction in scanning phased array antennas with large element spacing. *IEEE Trans Antennas Propag*. 2018;66(12):6965-6974.

[17] Iqbal Z, Pour M. Exploiting higher order modes for grating lobe reduction in scanning phased array antennas. *IEEE Trans. Antennas Propag*. 2019;67(11):7144-7149.

[18] Inserra D, Xie F, Yang Z, Huang Y, Li J, Wen G. Dual-mode microstrip patch antennas for largely spaced phased arrays. In: Proc. IEEE CSRSWTC; 2020

[19] Pinchera D, Migliore MD, Schettino F, Panariello G. Antenna arrays for line-of-sight massive MIMO: half wavelength is not enough. *Electronics*. 2017;6(3):57.

[20] Pinchera D, Migliore MD, Schettino F. Optimizing antenna arrays for spatial multiplexing: towards 6G systems. *IEEE Access*. 2021; 9:53276-53291.

[21] Anjos EVP, SalarRahimi M, Rehammar R, Schreurs DMMP, Vandenbosch GAE, Geurts M. A 5G active antenna tile and its characterization in a reverberation chamber. In: Proc. 14th EuCAP; 2020:1-4.

[22] Aslan Y, Puskely J, Janssen J, Geurts M, Roederer A, Yarovoy A. Thermal-aware synthesis of 5G base station antenna arrays: an overview and a sparsity-based approach. *IEEE Access*. 2018;6: 58868-58882.

[23] Sharma S, Shafai L, Balaji B, Damini A, Haslam G. Investigations on multimode microstrip patch antenna and phased arrays providing multiphase centres. In: 1A of Proc. IEEE APS-URSI; 2005.

[24] Garg R, Bhartia P, Bahl IJ, Ittipiboon A. *Microstrip antenna design handbook*. Norwood, Massachusetts: Artech House. 2001;73-126.

[25] Kishk A, Shafai L. The effect of various parameters of circular microstrip antennas on their radiation efficiency and the mode excitation. *IEEE Trans. Antennas Propag*. 1986;34(8):969-976.

[26] Lobo M, Vandenberghe L, Boyd S, Lebret H. Applications of second-order cone programming. *Linear Algebra Appl*. 1998; 284(1–3):193-228.

[27] Kuo YJ, Mittelmann H. Interior point methods for second-order cone programming and OR applications. *Computat Optim Appl*. 2004;28(3):255-285.

[28] Grant M, Boyd S. CVX: Matlab Software for Disciplined Convex Programming, version 2.1; 2014.

[29] Allahgholi PZ. Control of Phase Centre and Polarization in Circular Microstrip Antennas [Master's thesis]. The University of Manitoba; 2006.